Engineering Structures 214 (2020) 110675

Contents lists available at ScienceDirect

Engineering Structures

journal homepage: www.elsevier.com/locate/engstruct

Dynamic load test on progressive collapse resistance of fully assembled precast concrete frame structures

Yun Zhou[a,b,c], Xiang Hu[c], Yilin Pei[c], Hyeon-Jong Hwang[d,*], Taiping Chen[c], Weijian Yi[c], Lu Deng[c,1]

[a] Hunan Provincial Key Lab on Damage Diagnosis for Engineering Structures, Hunan University, Changsha 410082, China
[b] Key Laboratory for Green & Advanced Civil Engineering Materials and Application Technology of Hunan Province, Hunan University, Changsha 410082, China
[c] College of Civil Engineering, Hunan University, Changsha 410082, China
[d] School of Architecture, Konkuk University, Seoul 05029, South Korea

ARTICLE INFO

Keywords:
Progressive collapse
Dynamic test
PC moment frame
Beam-column joint
Dowel bar
Column removal
Finite element analysis

ABSTRACT

The progressive collapse of reinforced concrete (RC) and precast concrete (PC) structures is one of the most critical failure scenarios and is consequently of great concern to the structural engineering community. In this study, two half-scale RC and PC moment sub-structures were designed to evaluate the progressive collapse performance under a sudden mid-column loss scenario. In the PC specimen, the beam-column connection was fully assembled using the dowel bars embedded in a corbel, and steel angle cleats were applied to the connection between the upper surface of the beam-end and column to further transmit the flexural moment. The beam-column joint was strengthened by horizontal hoops and U-shaped bars. The dynamic responses such as the load-carrying capacity, beam deflection, lateral displacement, failure modes, crack distribution, and rebar strains were evaluated. The test results showed that the load-carrying capacity of the PC specimen was 76.9% of that of the RC specimen, while the ultimate deflection of the mid-column in the PC specimen was 106.1% of that of the RC specimen. Ultimately, shear failure occurred in the dowel bar connection of the PC specimen. On the other hand, ductile failure occurred by fracture of beam rebars in the RC specimen. Under dynamic loading, compressive arch action (CAA) was developed in the both specimens, but the effective catenary action (CTA) was developed in the RC specimen only. Finite element analysis was performed, and the analysis results agreed well with the test results. The dynamic test results and analysis results showed that the RC specimen exhibited better progressive collapse performance than the PC specimen.

1. Introduction

Since the collapse of London's Ronan Point apartment block in 1968, progressive collapse resistance of multi-story structures has been widely studied. Progressive collapse is defined as the spread of an initial local failure from element to element that eventually results in collapse of an entire structure or a disproportionately large part of it [1,2]. Disproportionate collapse may occur in a building when the structure is exposed to unexpected loadings caused by natural disasters, accidental explosions, or terrorist attacks [3,4]. For investigating structural solutions to prevent progressive collapse, the Alternate Load Path (ALP) approach has been widely used to analyse the resistance mechanisms, including compressive arch action (CAA), catenary action (CTA), and the contribution of infill walls [5]. Although the majority of current studies implemented quasi-static methods, nonlinear dynamic behavior needs to be considered to accurately predict the behavior of structures under a sudden-column-removal scenario [6].

A series of policies have recently been promulgated to rapidly develop precast concrete (PC) residential structures in China. Compared to on-site casting of reinforced concrete (RC) structures, PC structures can improve the construction quality, material performance control, and structural efficiency, as well as reduce on-site labour costs. For fast construction of the assembled PC moment frames, dry connections, such as welding connections, J-typed bolts connections, dowel rebar connections, tie rods, and angle cleat connections have been widely used [7–12]. However, compared to RC and PC wet connections, PC dry

* Corresponding author.
E-mail addresses: zhouyun05@gmail.com (Y. Zhou), baren@hnu.edu.cn (X. Hu), yilin_pei@hnu.edu.cn (Y. Pei), hwanggun85@naver.com (H.-J. Hwang), 1587536480@qq.com (T. Chen), wjyi@hnu.edu.cn (W. Yi), denglu@hnu.edu.cn (L. Deng).
[1] Co-corresponding author.

https://doi.org/10.1016/j.engstruct.2020.110675
Received 19 February 2019; Received in revised form 16 April 2020; Accepted 16 April 2020

connections are vulnerable to progressive collapse because of the discontinuity of the longitudinal reinforcement in the beam connections; under a column removal scenario, horizontal loads imposed by CAA and CTA may lead to column or joint failure. Further, the structural performance in terms of strength, flexibility, stability, energy dissipation capacity, displacement ductility, and residual forces, is significantly affected by the structural performance of dry connections [13].

In PC structures, the structural performance of connections is critical and has the greatest influence on the safety of the structure. Particularly for fully assembled PC structures, the PC frame cannot offer the same ductility as monolithic construction because of a lack of continuity in the PC joints; performance of a PC frame is concerned more with structural stability, robustness and integrity. While the ability of RC structures to resist progressive collapse has been investigated extensively, very little research has focused on PC structures subject to a single column removal scenario. Nimse et al. [14,15] performed a progressive collapse test for three 1/3 scale PC moment frames using concrete corbel or steel billet and found that the strength degradation of a dry precast connection was more significant than that of a monolithic connection. Tohidi et al. [16] contended that an underestimated tensile tie force would cause an unsafe design in PC floor joints in the absence of underlying wall supports. On the basis of experimental and computational studies of moment frames under a column removal scenario, Main et al. [17] reported that fractures of the anchorage bars occurred by the out-of-plane bending moment due to the transfer of eccentricity forces. Kang and Tan [18,19] evaluated the effects of a 90° hook and lap-splice of beam bottom bars in beam-column connections on the progressive collapse performance of a PC sub-structure under quasi-static loading. Results of the tests showed that the enhancement of CAA and CTA was affected by the joint details and beam rebar ratio. Qian and Li [20] tested a 1/3 scale RC beam-slab sub-structure and two 1/3 scale PC sub-structures with welded-connections and pinned-connections. Test results showed that the PC specimen with pinned connections showed better progressive collapse resistance compared to the PC specimen with welded connections. Feng et al. [21] considered the beam bar-slip at the beam-column joint to simulate the progressive collapse behavior of PC sub-assemblages in the *OpenSees* program. They found that the bar-slip decreased the load-carrying capacity of CAA and increased the rotation capacity of beam ends. According to Yu et al. [22], the load transfer mechanisms of beam-slab substructures is developed by CAA of longitudinal beams and the flexural mechanism of transverse beams at small deflection, and by CTA of beams as well as tensile membrane action of slabs at large deflection. Current static test results indicate that discontinuity of beam flexural bars in joints result in poor performance of CAA and CTA in PC structures. Further, for better evaluation of progressive collapse resistance in PC structures, nonlinear static analysis procedures incorporating equivalent dynamic factors is usually preferred in practice based on the energy balance method [23], while nonlinear dynamic behaviour needs to be studied for verification by the dynamic free-fall test.

Compared to studies on quasi-static pushdown tests, very few dynamic free-fall tests have been conducted because of the complicated test setup and mechanism required [24]. Sasani et al. [25] studied the dynamic performance of a RC building with one-way floor slabs after the sudden removal of an exterior column. Qian and Li [26] investigated the dynamic load redistribution of six 1/3 scale RC substructures with different design details, span length, and span aspect ratio under predefined initial damage, and found that progressive collapse resistance was significantly affected by the span length and seismic details. Yu et al. [27,28] compared the progressive collapse performance between seismic and non-seismic details in 1/2 scale RC sub-assemblages, and investigated the dynamic increase factor (DIF) and the dynamic load amplification factor (DLAF) of rebars. Orton and Kirby [29] performed dynamic tests on a 1/4 scale 2-story RC frame under a mid-column removal scenario to evaluate the dynamic responses and investigate the consequences of the snap-through effect. Pham et al. [24] found that CTA prevented progressive collapse in RC sub-frames under blast pressure, and that the stiffness of horizontal restraints affected to mitigate disproportionate collapse under both static and blast conditions. Pham et al. [30] performed dynamic loading tests on RC beam-column frames simulating the sudden removal of a supporting column, and compared the damage patterns and failure modes between the dynamic tests and static tests. Qian and Li [31] reported that the damage caused by dynamic response decreased initial stiffness and efficiency of CAA, as well as causing compressive membrane action in specimens under an elastic dynamic response. Qian et al. [32] quantified the dynamic load redistribution of flat-slab structures subjected to different extents of initial load damage by testing two multi-panel RC flat-slab substructures. Qian et al. [33] tested four 1/2 scaled unbonded post-tensioned precast concrete (UPPC) beam-column substructures under both quasi-static and dynamic loading regimes; the test results indicated that UPPC frames achieved the required load redistribution capacity to mitigate progressive collapse. Feng et al. [34] investigated the effects of static and dynamic loadings on the progressive collapse resistance of PC beam-column substructures. However, the majority of existing studies focused on the dynamic behaviour of RC structures. Since the discontinuity of beam flexural bars in joints may result in different dynamic responses and failure modes, a dynamic loading test and analysis needs to be performed for PC structures with various design conditions. For convenient design and evaluation of progressive collapse performance, DIF has been utilized to evaluate the relationship between the linear behaviour and nonlinear static behaviour as well as nonlinear dynamic behaviour. McKay et al. [35,36] proposed that the DIF and load increase factors be used to approximately account for the dynamic effects and to evaluate the progressive collapse performance. Ferraioli [37] studied the DIF value in RC frame buildings subjected to sudden loss of a first-story column.

Studies on PC structures under column-removal scenarios have found that different types of beam-column connections may significantly affect the failure mode, ductility, and integrity of PC structures. In addition, the dynamic effect should not be ignored when the progressive collapse behaviour of PC building structures is evaluated. This study presents the finite element analysis (FEA) results of experiments on two half-scale RC and fully assembled PC sub-structures. The connections are the key components in maintaining the structural integrity necessary for preventing progressive collapse. In a fully assembled PC connection, the conventional dry connection is regarded as a semi-rigid connection when the top stiffened channel is instrumented. To the best of the authors' knowledge, dynamic tests on a large-scale PC frame structure with fully-assembled semi-rigid connection has seldom been conducted. Thus, the dynamic behaviour of a PC structure with dry connections needs to be studied in order to accurately evaluate its progressive collapse performance.

In general, the vertical resistance of semi-rigid PC structures would be less than that of RC structures. The main purpose of this study is to compare the dynamic responses between a semi-rigid PC specimen and a RC specimen. In order to provide a complete insight into the dynamic effects on the structural responses, a series of dynamic tests with increased applied weights on the beams were carried out using free-fall release procedures. The progressive collapse performance (i.e., deformation capacity, failure modes, crack distribution, and rebar strain) is discussed and the load transfer mechanism compared. Three-dimensional FE simulations were also conducted using the ABAQUS program. The successful calibration of the FE model resulted in a rational estimation of the target response without residual damage.

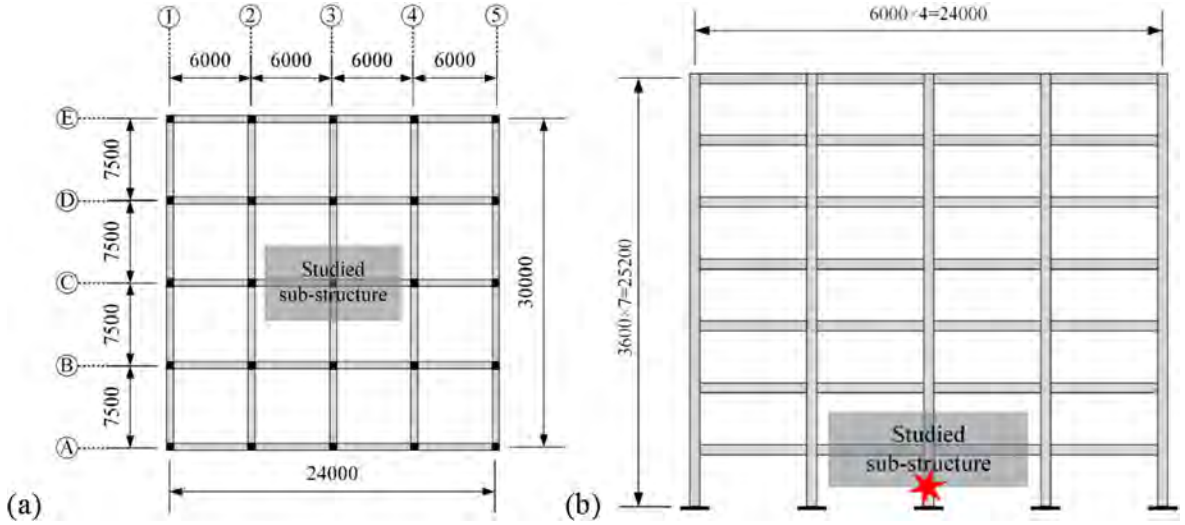

Fig. 1. Details of prototype building: (a) plane view; (b) elevation view (unit: mm).

2. Specimen design

2.1. Design of prototype structure

In order to explore the progressive collapse performance of fully assembled PC frame structures, a four-span 7-story frame structure was designed according to the *Code for Design of Concrete Structures* [38] and the *Code for Seismic Design of Buildings* [39]. Fig. 1 shows the prototype of test specimens. The floor height was 3.6 m, and the span was 6 m and 7.5 m in x- and y- directions respectively. Design dead and live loads were 5.0 kN/m^2 and 2.0 kN/m^2, respectively. Seismic intensity was classified as degree 7, and the design basic earthquake acceleration T_g was defined as 0.1 g according to Chinese design code GB 50011-2010 [39]. The field category was defined as class 2, which refers to a field with a mean shear wave velocity, V_{30} , of between 260 m/s and 510 m/s in accordance with the relevant US code [40]. An interior sub-frame was considered as a test specimen to investigate the load transfer path and failure mechanism under the removal of the mid-column by accidental loads. The specimen design was based on the results of a three-dimensional *PKPM* analysis [41]. Considering a semi-rigid boundary condition of the actual PC joint, the maximum moment in both cases of the fully fixed and hinged boundary conditions was used in the specimen design.

2.2. Design of test specimen

To consider a larger rotation of a short span beam under the same deflection in laboratory conditions, a span of 6 m was tested; for simplification, the resistance of the 3D space effect from the slab and crossbeams was ignored. Fig. 2 and Table 1 show the details of two test specimens that consist of two span beams and three columns with the mid-column removed. The cross-sectional area of the beam sections was 200 mm × 300 mm, and the two 3000 mm high exterior columns had a cross-sectional area of 350 mm × 350 mm. The height of the columns between the footing and lateral support was 2700 mm. In the RC specimen, four T18 bars (diameter = 18 mm and cross-sectional area = 254.5 mm^2) and eight T16 bars (diameter = 16 mm and cross-sectional area = 201.1 mm^2) were used for longitudinal bars of the beams and columns, respectively. R6 bar (diameter = 6 mm and cross-sectional area = 28.3 mm^2) was used for transverse reinforcement at a spacing of 50 mm in the plastic hinge region of the beam and column. In the beam-column joint, R6 bar was placed at a spacing of 40 mm. A conventional connection was designed for the beam-column joint with continuous longitudinal bars. In the fully assembled PC specimen, the identical geometric dimensions and reinforcement details were used, except for the connection of the beam-column joint. Two dowel bars of 20 mm diameter projected from the corbel of the precast column were inserted into two dowel sleeve holes of 40 mm diameter embedded in the precast beam end. The steel angle cleat stiffened with three side plates was installed on the top face of the beam end to further improve the load transfer capacity. The projected dowel bars were bolted at the steel angle cleat, and high-strength bolts passed through the column to connect the steel angle cleat. Horizontal U-shaped bars were used in the beam end and corbel for anchorage of the beam longitudinal bars and dowel bars, respectively. Gaps and holes in the specimen were filled with non-shrink high-strength grouting material. Table 2 shows the material properties.

3. Test program

3.1. Test setup

Fig. 3 shows the test setup of the specimens. Fixed boundaries were established at the footing, and the top of the column was simply supported by a load cell. Steel frames were used to prevent the out-of-plane movement of the specimens. Using a quick-release device, the sudden column-removal process was simulated for the dynamic test [30]. Four 1900 mm × 900 mm × 700 mm baskets of various weights were suspended along the beam to equivalently simulate the actual uniform load distribution (Fig. 3(a)). The detailed test setup used in this study simulates the actual load situation better than that of many existing studies, except those of Qian and Li [26], Orton and Kriby [29], Liu et al. [42]. Rubber gaskets were used at the interface between the steel strands and beam to avoid concrete crushing damage.

3.2. Instrumentation layout

Fig. 4 shows the layout of the measurement devices to measure the dynamic response of the test specimens. The reaction forces of the mid-column and exterior columns were measured by load cells with a capacity of 100 kN and 300 kN, respectively. Two transducers (800 mm range) were used to measure the deflections of the mid-column and mid-span of a right-side beam, and four transducers (160 mm range) were used to measure the lateral displacement of the exterior columns. Four accelerometers were arranged at the top of the mid-column as well as the mid-span of a beam and the exterior joints. The dynamic data was acquired at a sampling frequency of 2400 Hz. In the RC specimen, 20 strain gauges were placed along the longitudinal bars of the beam/

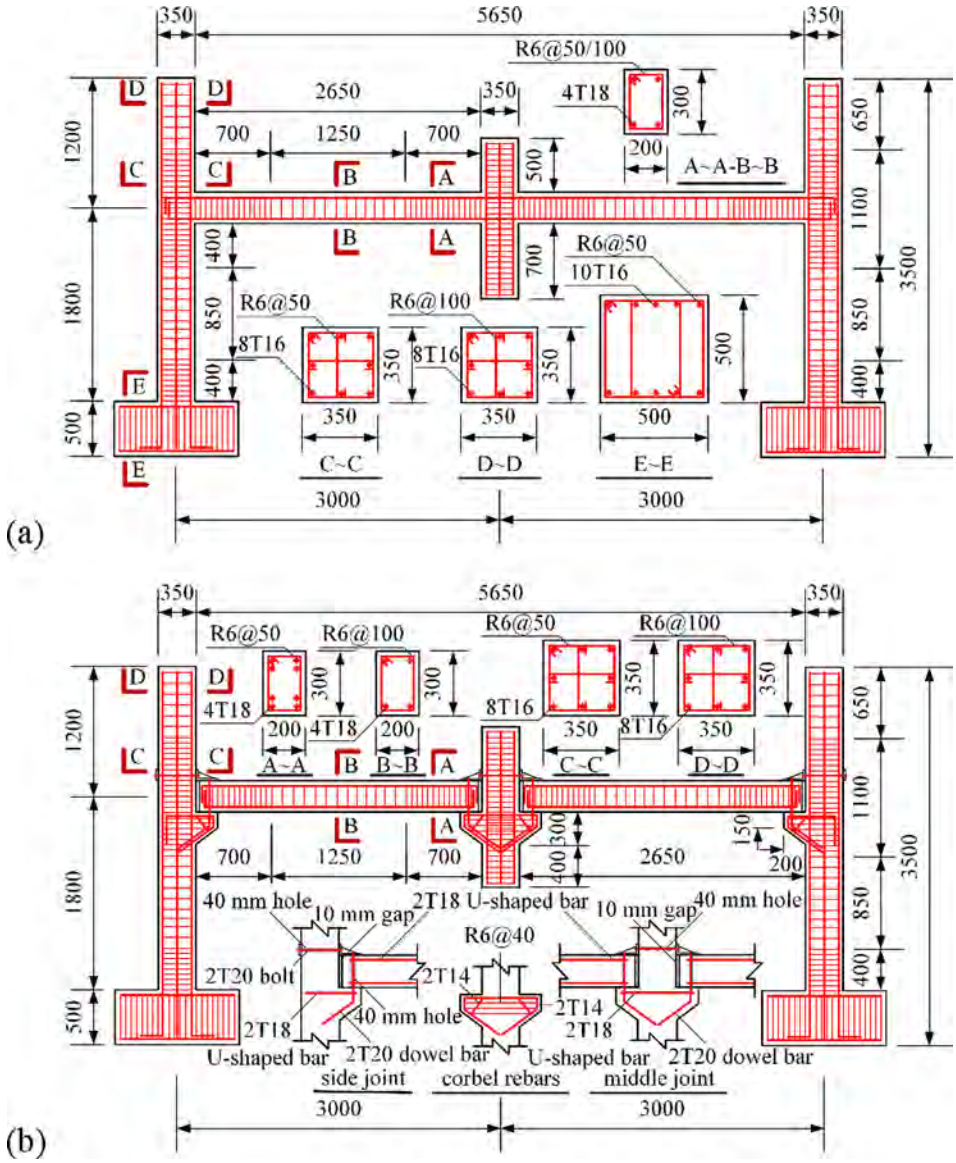

Fig. 2. Cross-sectional details of test specimens: (a) RC specimen; (b) PC specimen (unit: mm).

column. In the PC specimen, 26 strain gauges were placed along the longitudinal bars of the beam/column and the dowel bars of the corbels. A high-speed camera with a sampling frequency of 1024 f/s was used to record the crack patterns and failure modes of the specimens.

3.3. Test procedures

The dynamic loading test consisted of following four steps.

Step 1: A specimen was pre-loaded by utilizing steel plates. During this process, a fixed hydraulic jack was placed at the bottom of the mid-column, and the initial axial force was measured by a load cell at the top of the mid-column. The dynamic factor was generally reported as around 1.2–1.3 according to a series of tests and analysis [28,30,43]. Each loading step was designed as 20%, 40%, 60%, 80%, and 100% of the peak strength under static loading with a dynamic factor of 1.3. Thus, the dynamic load under 80% of 1.3 factor is almost the same as 100% of the static peak strength, and the dynamic load under 100% of 1.3 factor can simulate the ultimate state for collapse of the PC/RC test specimens. Meanwhile, 1 kN load was added to each basket at the 1st load step to evaluate the elastic behavior, and then 10 kN was added to each basket in the next load steps. Due to the limited amount of steel plates, the steel plates were added to two baskets near the mid-column

Table 1
Specimen details (unit: mm).

Specimens	Dimensions				Longitudinal bars			Transverse bars		
	Column section ($b \times h$)	Column height (H)	Beam section ($b \times h$)	Beam length (L)	Column	Beam	Joint	Column	Beam	Joint
RC	350 × 350	3000	200 × 300	2650	8 T16	4 T18	–	R6@50/100	R6@50/100	–
PC	350 × 350	3000	200 × 300	2630	8 T16	4 T18	4 T14			R6@40

Note: T16 denotes the deformed bar with 16 mm diameter, and R6 denotes the plain bar with 6 mm diameter.

Table 2
Material properties.

Materials	Types	Yield strength (MPa)	Tensile strength (MPa)	Elongation (%)
Reinforcing bars	R6	385	460	δ_5 = 26%, δ_{10} = 21%
	T14	465	616	δ_5 = 25%, δ_{10} = 22%
	T16	505	630	δ_5 = 28%, δ_{10} = 23%
	T18	485	622	δ_5 = 24%, δ_{10} = 21%
	T20	493	629	δ_5 = 27%, δ_{10} = 19%
Concrete	RC: Cube (150 mm × 150 mm × 150 mm): 27.4 MPa; Cylinder ($D \times L$ = 150 mm × 300 mm): 24.7 MPa			
	PC: Cube (150 mm × 150 mm × 150 mm): 37.6 MPa; Cylinder ($D \times L$ = 150 mm × 300 mm): 28.3 MPa			
Grouting	PC: Cube (100 mm × 100 mm × 100 mm): 43.4 MPa			

Note: δ_5 and δ_{10} indicate the elongation of the tensile bar with tagging length of 5- and 10-times diameter, respectively.

at the 5th and 6th load steps.

Step 2: A quick-release device was connected to the top of the mid-column after the pre-loading process, and then the bottom hydraulic jack was removed.

Step 3: The quick-release mechanism was applied to simulate the sudden column-removal process. Thus, the transient dynamic response could be measured.

Step 4: The released mid-column was moved upward to the original location by the hydraulic jack, and the next load step with increased weight was then applied until the specimen failed.

4. Test results

Table 3 shows the load conditions for the dynamic loading test. As shown in Fig. 5, the PC specimen failed at the 4th load step, while the RC specimen failed at the 6th load step. The release time was kept within 0.020–0.030 s except for the 1st and 2nd load steps, because the release time was affected by the weight of applied loads as well as the human-controlled pulling out of the pin rod on the quick-release device.

The RC specimen did not immediately collapse at the end of the 6th load step (Fig. 6). Fig. 7(a) shows the crack distribution in the RC specimen. Concrete crushing slightly occurred on the top surface close to the interior beam-column joint, and cracks appeared on the surface of both sides of the beam (Fig. 8).

After 20 min under a sustained load, an unexpected failure of the RC specimen occurred without warning as shown in Fig. 7(b). The beam top bars at the joint interface of the right exterior beam-column joint were fractured, and shear failure occurred at the beam end near the left exterior beam-column joint, which increased the deflection of the mid-column to 490 mm. However, the RC specimen did not completely collapse due to CTA. The number of cracks and the crack width significantly increased, and concrete crushing occurred at the joint interface of the interior beam-column joints (Fig. 9).

Such phenomenon may indicate that the sustained load was the critical load from beneficial action to adverse action between CAA and CTA as shown in Fig. 10. The sustained load caused the creep of concrete, which increased the deflection gradually until a critical point. Unfortunately, that particular test data was not well recorded because the phenomenon was unexpected.

4.1. Time-deflection relationship

Fig. 11 and Table 4 show the deflection responses of the mid-column and mid-span of a right-side beam. The secant stiffness was calculated at the peak deflection of the mid-column. The dynamic amplification factor (DAF) is conventionally defined as the ratio of the maximum dynamic displacement to the static displacement for an elastic SDOF system under an applied loading (displacement-based DAF), which is also known as 'dynamic magnification factor' [44] or 'displacement response factor' [45]. For the specimen utilized in the dynamic test, the PC beams were connected to PC columns by using dowel bars and a steel angle cleat, which can be regarded as a semi-rigid joint. Meanwhile, the RC specimen joint can be regarded as a rigid joint. According to the comparative quasi-static pushdown tests on the same RC and PC specimens [46], the vertical yield stiffness were 1.47 kN/mm and 3.92 kN/mm for PC and RC specimens, respectively.

Compared with the RC specimen, the PC specimen exhibited a larger deflection, vibration amplitude, and natural period, which was consistent with the static test results because of the lower vertical stiffness in the assembled PC structure [46]. The natural period of test specimens was identified by picking the average peak values in the decayed deflection history of Fig. 11. When the wavelength was not quite clear, the natural period of vibrations measured from the accelerometers was used.

When compared to the 1st load step, in the PC specimen under the 2nd load step, the peak deflections of the mid-column and beam mid-

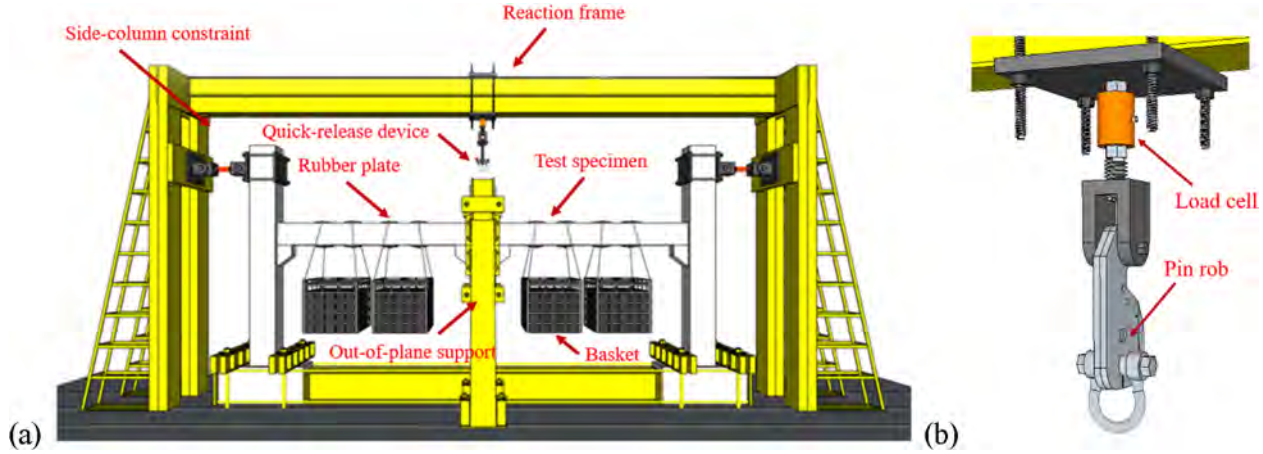

Fig. 3. Test setup: (a) boundary conditions; (b) quick-release device.

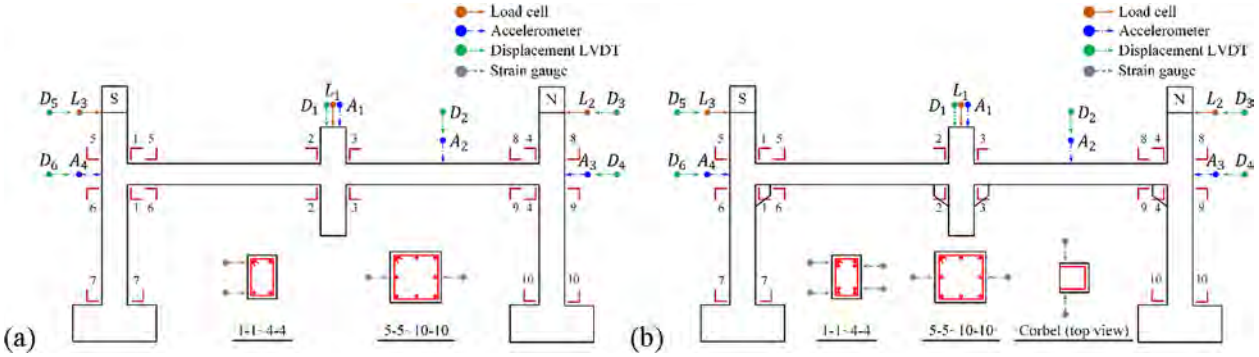

Fig. 4. Instrumentation layout: (a) RC specimen; (b) PC specimen.

span increased by 13.0 mm and 5.6 mm, respectively, while the secant stiffness decreased by 5.7% (Fig. 11(b)). The natural period increased by 58% due to the mass increase and stiffness degradation. In the RC specimen, the peak deflections of the mid-column and beam mid-span increased by 4.4 mm and 2.6 mm, respectively, while the secant stiffness decreased by 36.1%; the natural period increased by 52.2%. As shown in Table 4, the same DAF of about 1.2 was measured during the test. This result indicates that the same loading mechanism was generated in both specimens. In the PC specimen under the 3rd load step, the peak deflections of the mid-column and beam mid-span increased by 34.0 mm and 17.6 mm, respectively (Fig. 11(c)). The secant stiffness decreased by 40.7%, and the natural period increased by 38.0%. On the other hand, the peak deflections of the RC specimen increased by only 5.2 mm and 2.9 mm, the secant stiffness decreased by 14.2%, and the natural period increased by 38.7%. This result indicates that the stiffness degradation of the RC specimen is less than that of the PC specimen. In the PC specimen under the 4th load step, the beam mid-span deflection was not measured due to a malfunction of the device channel. The ultimate deflection of the mid-column reached 522.2 mm, which was 9 times that of the 3rd load step (Fig. 11(d)). In the RC specimen, the peak deflections of the mid-column and beam mid-span increased by 7.4 mm and 6.5 mm, respectively. The secant stiffness decreased by 22.0%, and the natural period increased by 18.9% (Fig. 11(e)). In the RC specimen under the 5th load step, the peak deflections of the mid-column and beam mid-span increased by 13.1 mm and 8.5 mm, respectively (Fig. 11(f)). The secant stiffness decreased by 22.5%, and the natural period increased by 16.8%. Under the 6th load step, the RC specimen exhibited plastic behaviour without transient vibration (Fig. 11(g)). The peak mid-column and beam mid-span deflections increased to 105.5 mm and 49.4 mm, respectively. The secant stiffness decreased to 1.08 kN/mm, which was a 65% decrease. In conclusion, the peak deflections of the mid-column and beam mid-span of PC and RC specimens increased as the load step increased. Before the PC specimen collapsed at the 4th load step, the peak deflection of the PC specimen was about 4 to 5 times that of the RC specimen. Further, as the load step increased, the residual deflection obviously increased, and the stiffness gradually decreased in the PC and RC specimens. In both specimens, the values of DAF were 1.05–1.30 without a clear rule. As the load step increased, damage accumulated in the specimens, which increased the natural period. The natural period of the PC specimen was larger than that of the RC specimen, which indicates a lower vertical resistance.

Fig. 5. Failure mode of specimens at the end of the 4th load step: (a) PC specimen; (b) RC specimen.

4.2. Lateral displacement of exterior columns

Figs. 12 and 13 show the lateral displacements of the exterior columns and joints in the PC and RC specimens, respectively. The positive and negative values indicate the inward and outward movements of the columns, respectively. Under the 1st load step, the lateral displacement of the PC specimen was relatively larger than that of the RC specimen,

Table 3
Load conditions.

Test ID	Applied loads					Pre-released force		Released time		Modified force	
	Pos. 1 (kN)	Pos. 2 (kN)	Pos. 3 (kN)	Pos. 4 (kN)	Total (kN)	PC (kN)	RC (kN)	PC (s)	RC (s)	PC (kN)	RC (kN)
1st	3.35	3.35	3.35	3.35	13.40	21.50	20.60	0.030	0.064	6.80	7.10
2nd	13.35	13.35	13.35	13.35	53.40	43.80	39.70	0.028	0.036	29.10	26.20
3rd	23.35	23.35	23.35	23.35	93.40	59.80	60.60	0.026	0.029	45.10	47.10
4th	33.35	33.35	33.35	33.35	133.40	81.10	76.80	0.020	0.021	66.40	63.30
5th	33.35	43.35	43.35	33.35	153.40	–	101.00	–	0.022	–	87.50
6th	33.35	53.35	53.35	33.35	173.40	–	114.30	–	0.019	–	100.80

Note: The modified force denotes the axial force of the mid-column contributed by the applied loads which eliminates the effect of specimen self-weight.

Fig. 6. Failure mode of RC specimen at the end of the 6th load step: (a) damage condition at the end of the test; (b) collapse condition after 20 min of the test.

but the amplitude was not significant (Figs. 12(a) and 13(a)). In the PC specimen under the 2nd load step, the peak lateral displacements of the beam-column joint and column were −0.82 mm and −0.44 mm, respectively (Fig. 12(b)). In the RC specimen, the peak lateral displacements of the beam-column joint and column were −0.30 mm and −0.19 mm, respectively (Fig. 13(b)). Under the 3rd load step, the peak lateral displacements of both specimens increased, showing a similar behaviour to those of the specimens under the 2nd load step. In the PC specimen under the 4th load step, an obvious change of the displacement direction occurred by temporary CTA (Fig. 12(d)). However, CTA was terminated due to failure of the beam-column joint, and the specimen ultimately collapsed. In the RC specimen under the 6th load step, the initial lateral displacement of the exterior columns was about −2.0 mm before the load was released (Fig. 13(f)). This is because the outward movement of the exterior columns occurred when the additional weight was applied for the dynamic test. After the load was released, the lateral displacements of the exterior joint and column were approximately −7.4 mm and −5.2 mm, respectively. However, after the RC specimen collapsed the lateral displacements of the exterior joint and column changed to 8.3 mm and 6.6 mm, respectively, as CTA developed.

4.3. Failure modes

In the PC specimen under the 1st load step, cracks were initiated in the beam-column joint and developed along the dowel bar. Cracks around the exterior and interior beam-column joints occurred first at the beam bottom and top, respectively. It is noted that this crack development differed from that under static load. In the RC specimen, cracks were initiated at the beam top of the exterior beam-column joint, which were distributed along the beam with equal distance interval. In the PC specimen under the 2nd load step, beam cracks were concentrated in the joint region, and developed along the dowel bar. Minor cracks occurred at the outside of the exterior columns due to the outward movement of the exterior columns. In the RC specimen, cracks were equally distributed at a spacing of 150 mm along the beam, and the crack length reached 150 mm. In the PC specimen under the 3rd load step, larger cracks occurred in beam-column joints, and the crack length reached 300 mm at the column section. Further, diagonal cracks occurred around the corbel and flexural cracks were initiated at the bottom of the exterior columns. In the RC specimen, the crack length was approximately 200 mm at the beam section, and flexural-shear cracks occurred in the beam end near the exterior columns. Further, flexural cracks occurred in the exterior column at a spacing of 150 mm, where the largest crack length was approximately 200 mm. The different crack patterns were attributed to the discrepancy of the load resistance in the both specimens.

Fig. 14 shows the failure modes of the left exterior beam-column joint in the PC specimen under the 4th load step. The specimen failed by shear failure of the dowel bar at the beam-column joint, and concrete crushing occurred in the beam-end and corbel under large deformation. Ultimately, both of the interior and exterior beam-column joints became geometrically unstable, and the temporary CTA was generated to resist the load.

In the RC specimen under the 4th load step, the number and length of cracks increased, and the crack passing through the beam section occurred. Further, more cracks occurred in the exterior columns and exterior beam-column joints, where the largest crack length was 300 mm. In the RC specimen under the 5th load step, the length and width of cracks in the beam further increased, while the number of cracks was maintained. However, more cracks occurred along the exterior column, and the crack length reached 350 mm.

Fig. 15 shows the dynamic response of the left beam-column joint in the RC specimen under the 6th load step. The crack width at the beam top face increased after the load was released, and concrete spalling occurred at the beam bottom. Ultimately, the major crack width increased to 10 mm at the beam end, and concrete crushing occurred at the beam top face near the interior beam-column joint. Flexural cracks were uniformly distributed in the exterior column, and diagonal cracks with a length of 400 mm were observed in the exterior beam-column joint. A few cracks occurred at the bottom of the exterior column. The initial shear cracks appeared at an early stage due to large shear force, because the steel strand used for hanging the steel basket was close to the beam-column joint interface. It may also be related to the accumulated damage in several steps. Under the collapse of the RC specimen, tensile fracture of the reinforcement occurred in the right beam, and shear failure occurred in the left beam. This complicated collapse procedure resulted from the fact that the shear force significantly increased in the left beam near the exterior joint, which was due to the load redistribution after the top bars of the right beam end near the exterior joint became fractured. The inward cracks occurred at the bottom of the exterior column, which showed that the specimen was affected by CTA. Both the test results and damage patterns revealed that the dynamic load was resisted at the critical state between CAA and

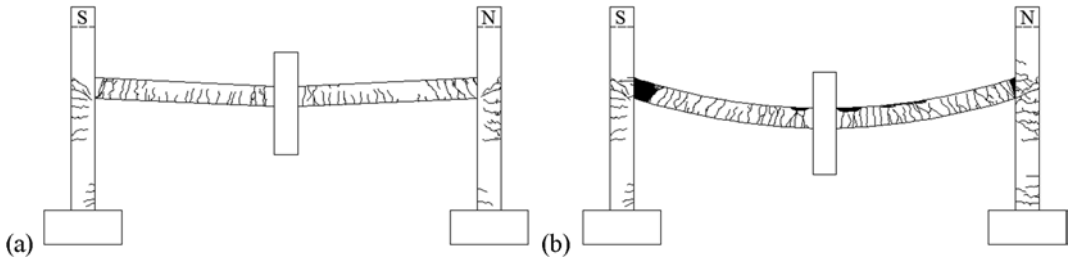

Fig. 7. Crack distribution of RC specimen: (a) damage condition at the end of the test; (b) collapse condition after 20 min of the test.

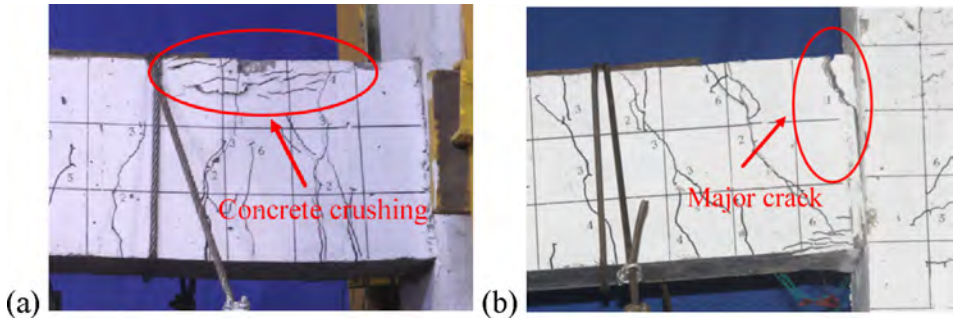

Fig. 8. Crack distribution of RC specimen at the end of the test: (a) interior beam-column joint; (b) right exterior beam-column joint.

CTA. CAA firstly developed as the outward displacement occurred in the exterior columns, but the effect was negated by the increase of the deflection and cracks. CTA developed under large deflection of the mid-column, which caused the inward displacement of the exterior columns.

4.4. Rebar strain

Fig. 16 shows the rebar strain distribution of the PC specimen under the 3rd load step. The peak strains of the beam longitudinal bars were 1862 με in tension and −2320 με in compression, which were close to the yield strain of 2425 με (Fig. 16(a)). The peak tensile strain of the U-shaped bar was 1504 με, and the peak compressive strain was −1455 με, which was less than the longitudinal bar strain (Fig. 16(b)). The axial force of the beam longitudinal bars was partly transmitted by the U-shaped beam-end bars, which strengthened the progressive collapse resistance of the PC specimen. The peak strains of the column longitudinal bars were 1737 με in tension and −210 με in compression (Fig. 16(c)). The column bar strain distribution shows that the exterior columns in the beam-column joint laterally moved in the outward direction (i.e., the load-carrying capacity is affected by CAA). The peak strains of the U-shaped bars in the corbel were 852 με in tension and −325 με in compression (Fig. 16(d)).

Fig. 17 shows the rebar strain distribution of the PC specimen under the 4th load step. The beam longitudinal bars yielded at the bottom of sections 2-2 and 4-4, showing the peak compressive strain of −3299 με. However, due to the lack of effective constraint mechanics in the beam-column joint during the collapse process, the tensile strength of the beam longitudinal bars was not fully developed, showing the peak strain of 1730 με (Fig. 17(a)). The strains of the U-shaped bars at the beam end significantly increased. Except for the bottom bars of sections 1-1 and 2-2 showing the malfunction of the strain gauges, the tensile strain of the bars was less than the yield strain, showing a peak tensile strain of 1982 με (Fig. 17(b)). The compressive strain at the top of section 2–2 and the bottom of section 4-4 exceeded the yield strain, showing the peak compressive strain of −7788 με. The peak strains of the column longitudinal bars were 2192 με in tension and −615 με in compression (Fig. 17(c)). The compressive/tensile strains of the column longitudinal bars were converted into tensile/compressive strains during the collapse process, as the load resistance mechanism changed from CAA to CTA. The peak strains of the U-shaped bars in the corbel were 1560 με in tension and −828 με in compression, which were less than the yield strain (Fig. 17(d)).

The rebar strain distribution of the RC specimen under the 4th load step is shown in Fig. 18. The top bars of the beam near the exterior beam-column joint yielded (i.e., the peak tensile strain = 4112 με), while the top bars of the beam near the interior joint did not yield (i.e., the peak compressive strain = -931 με). The peak strains of the column longitudinal bars were 825 με in tension and −645 με in compression (Fig. 18(b)). Unlike the PC specimen that collapsed under the 4th load step, the RC specimen resisted a larger load.

The rebar strain distribution of the RC specimen under the 6th load step is shown in Fig. 19. The top bars of the beam near the mid-column yielded without transient vibration (Fig. 19(a)). Further, the column longitudinal bar yielded in tension (i.e., the peak tensile strain = 2806 με), and the peak compressive strain significantly increased to −1271 με.

5. Finite element analysis

For test specimens under several dynamic loads, residual damage is unavoidable. In order to investigate the residual damage, FEA was performed using the *ABAQUS/Explicit* program, in which residual damage is not considered. Thus, the extent of the residual damage was evaluated by comparing the analysis results with the test results. The dynamic load transfer mechanism of two specimens subjected to the mid-column removal scenario was also investigated.

5.1. Element types

Fig. 20 shows the analysis model of PC and RC specimens. An eight-node solid element with reduced integration (C3D8R) was employed to simulate the concrete of beams, columns, and corbels, while a two-node truss element (T3D2) was employed to simulate reinforcing bars. The beam element is compatible with solid elements considering computational efficiency and robustness. A convergence study was carried out by trial and error calculation, and the mesh size of concrete elements

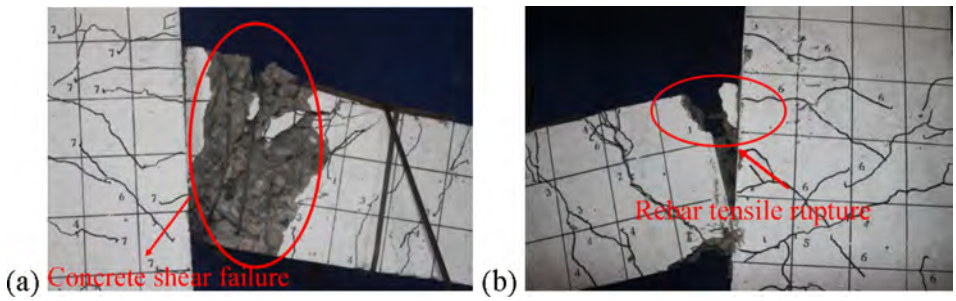

Fig. 9. Crack distribution of RC specimen after 20 min of the test: (a) interior beam-column joint; (b) right exterior beam-column joint.

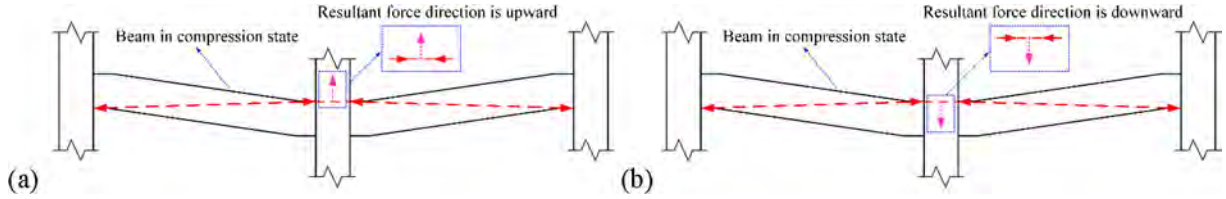

Fig. 10. Schematic diagram of beneficial and adverse compressive arch actions: (a) beneficial action; (b) adverse action.

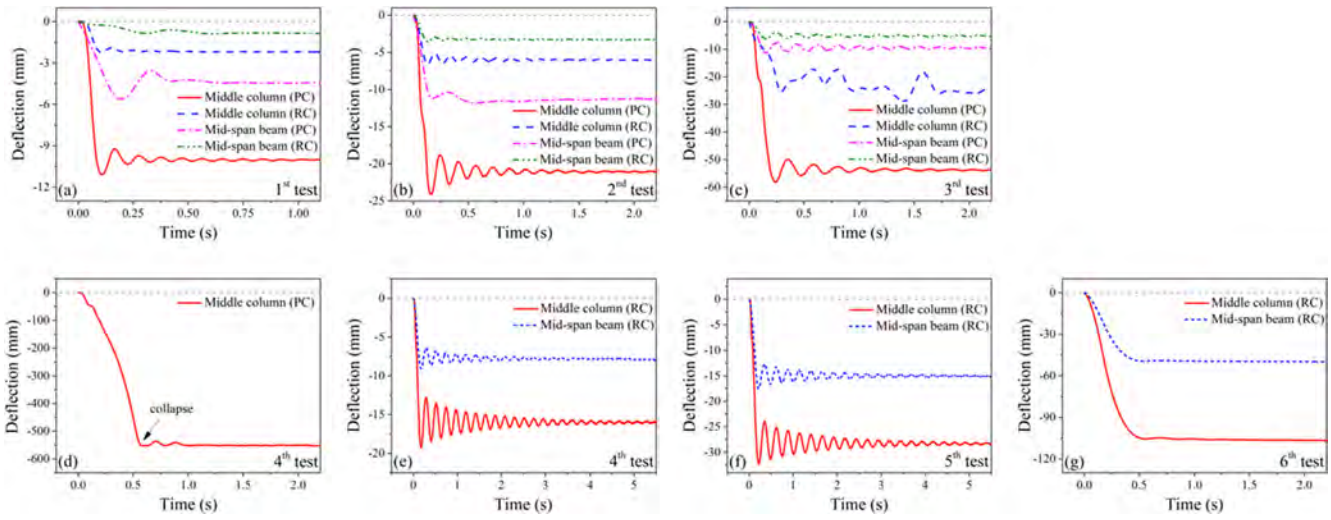

Fig. 11. Deflection history of test specimens: (a) 1st load step; (b) 2nd load step; (c) 3rd load step; (d) 4th load step of PC specimen; (e) 4th load step of RC specimen; (f) 5th load step; (g) 6th load step.

Table 4
Test results.

Test ID	Type		Peak defl. (mm)	Residual defl. (mm)	Stiffness (kN/mm)	DAF	Response time (s)	Natural period (s)
1st	PC	Column	−11.1	−10.0	1.93	1.11	0.076	0.100
		Beam	−5.6	−4.4		1.27	0.164	
	RC	Column	−2.2	−2.1	9.36	1.05	0.004	0.090
		Beam	−0.9	−0.8		1.13	0.240	
2nd	PC	Column	−24.1	−21.1	1.82	1.14	0.131	0.158
		Beam	−11.2	–		–	0.137	
	RC	Column	−6.6	−6.0	5.98	1.11	0.094	0.137
		Beam	−3.5	−3.3		1.06	0.091	
3rd	PC	Column	−58.1	−53.7	1.03	1.08	0.207	0.218
		Beam	−28.8	–		–	–	
	RC	Column	−11.8	−9.5	5.13	1.24	0.115	0.190
		Beam	−6.4	−5.2		1.23	0.115	
4th	RC	Column	−19.2	−16.0	4.0	1.20	0.150	0.226
		Beam	−9.1	−7.8		1.16	0.152	
5th	RC	Column	−9.1	−28.2	3.1	1.15	0.194	0.264
		Beam	−32.3	−15.0		1.17	0.189	

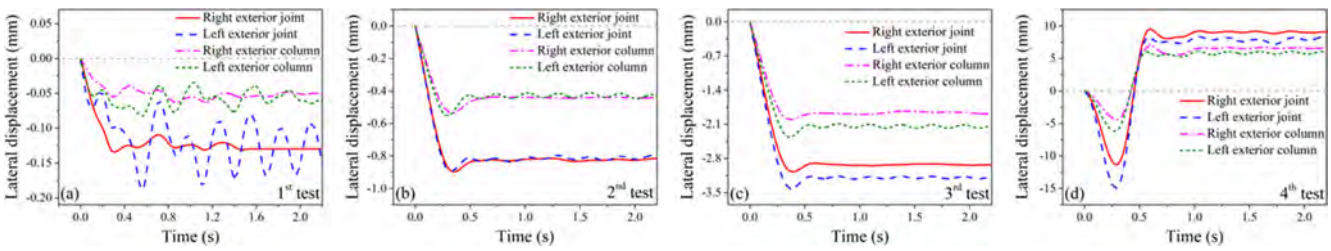

Fig. 12. Lateral displacements of the exterior columns and joints in PC specimen: (a) 1st load step; (b) 2nd load step; (c) 3rd load step; (d) 4th load step.

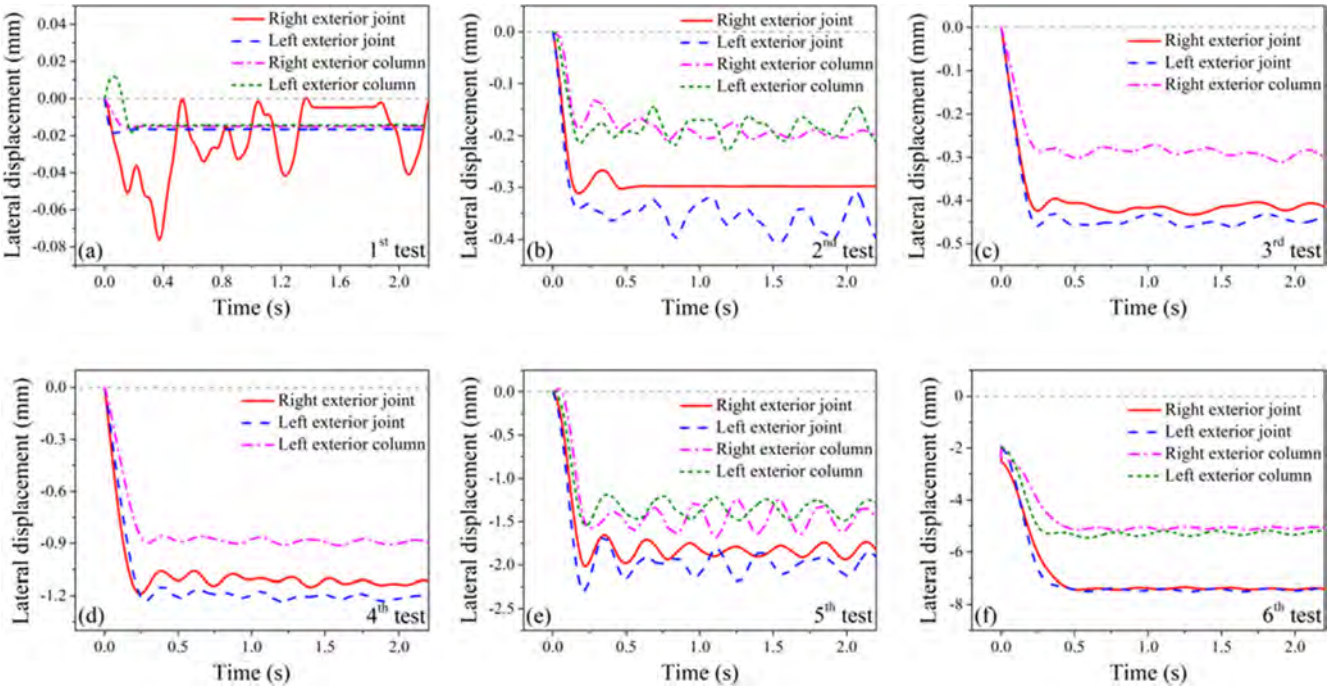

Fig. 13. Lateral displacements of the exterior columns and joints in RC specimen: (a) 1st load step; (b) 2nd load step; (c) 3rd load step; (d) 4th load step; (e) 5th load step; (f) 6th load step.

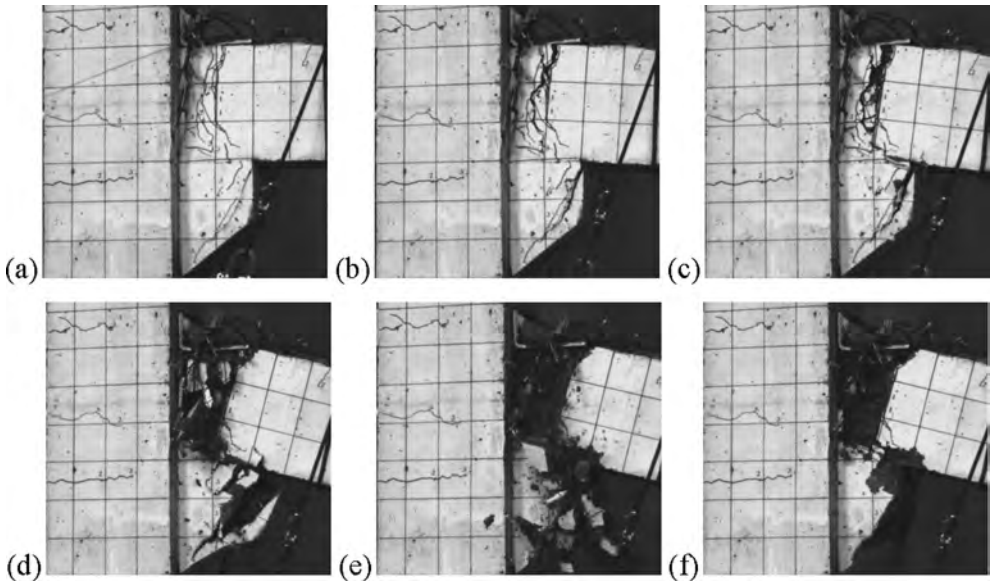

Fig. 14. Failure modes of left beam-column joint in PC specimen under the 4th load step: (a) t = 0 ms; (b) t = 140 ms; (c) t = 280 ms; (d) t = 420 ms; (e) t = 560 ms; (f) t = 1120 ms.

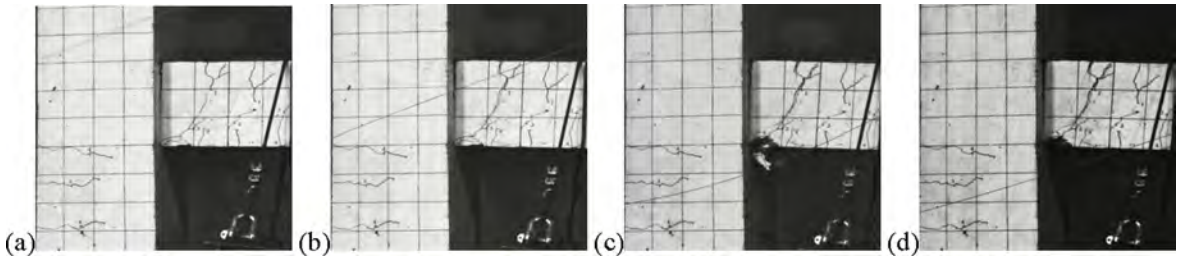

Fig. 15. Failure modes of left beam-column joint in RC specimen: (a) t = 0 ms; (b) t = 140 ms; (c) t = 280 ms; (d) t = 560 ms.

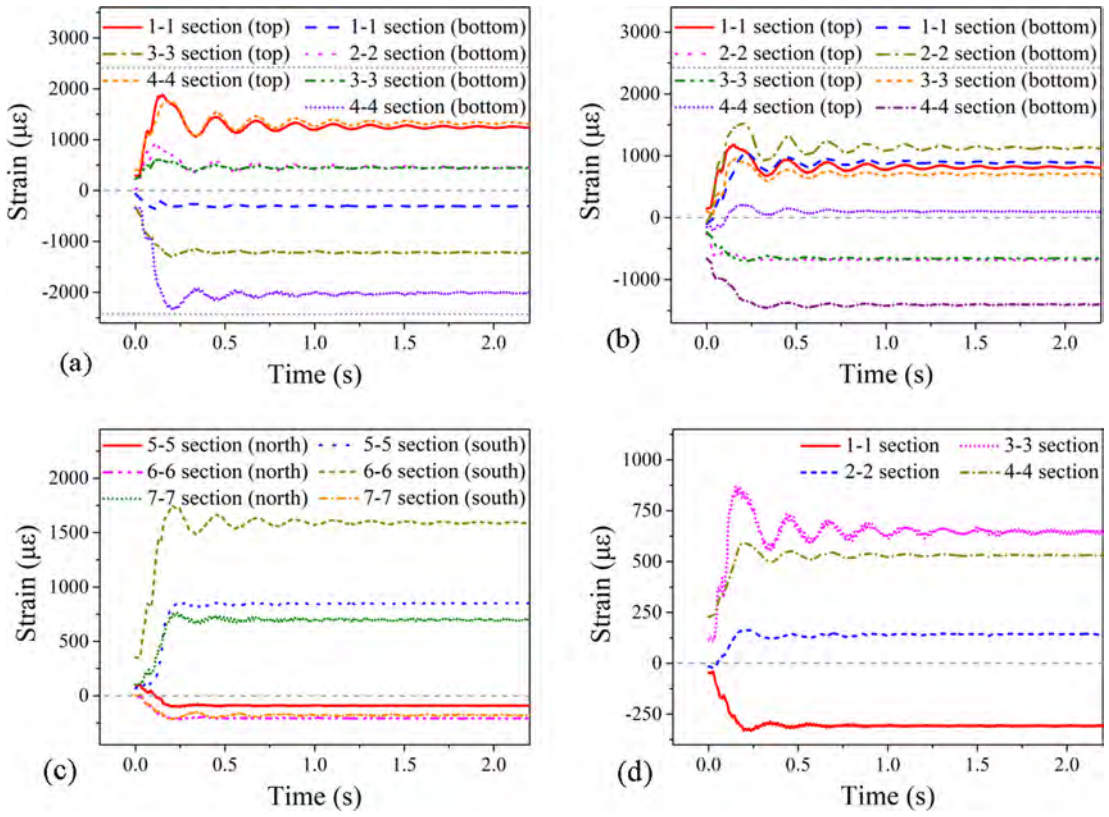

Fig. 16. Rebar strain of PC specimen under the 3rd load step: (a) beam longitudinal bars; (b) U-shaped bars of beam-end; (c) column longitudinal bars; (d) U-shaped bar of corbel.

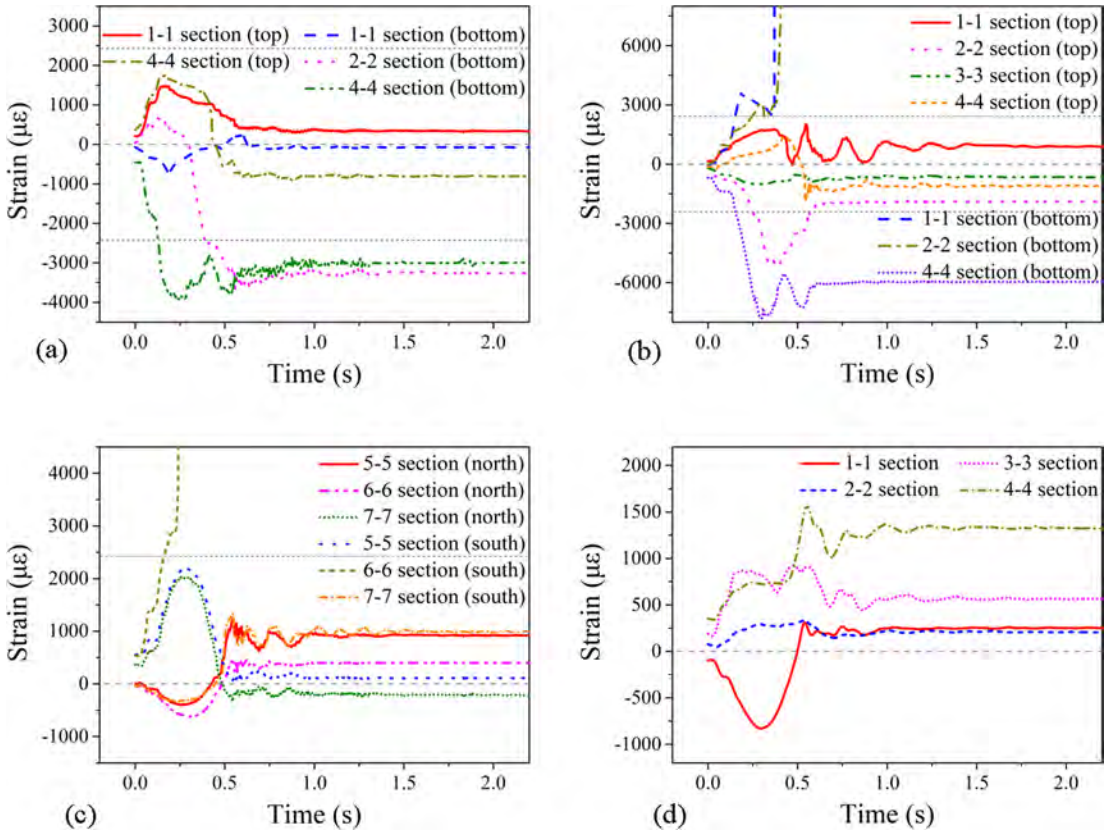

Fig. 17. Rebar strain of PC specimen under the 4th load step: (a) beam longitudinal bars; (b) U-shaped bars of beam-end; (c) column longitudinal bars; (d) U-shaped bar of corbel.

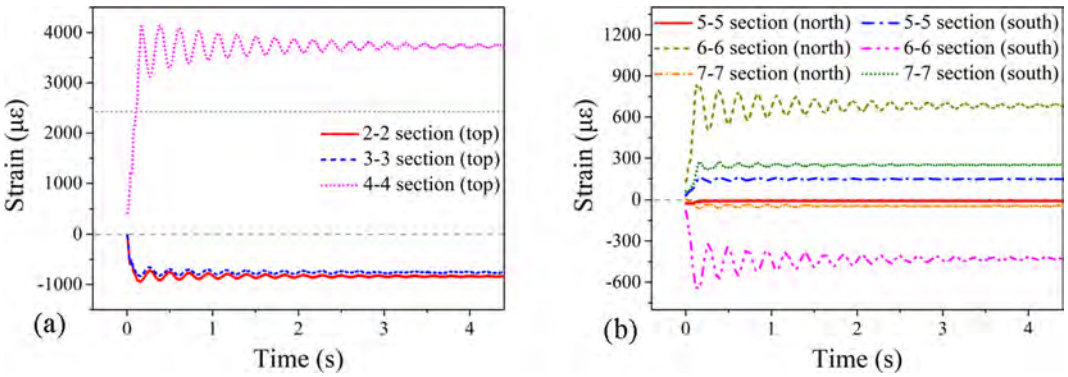

Fig. 18. Rebar strain of RC specimen under the 4th load step: (a) beam longitudinal bars; (b) column longitudinal bars.

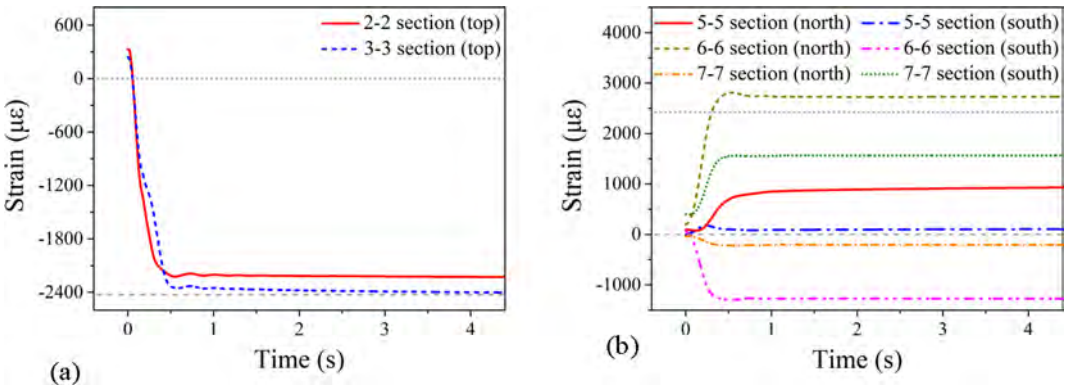

Fig. 19. Rebar strain of RC specimen under the 6th load step: (a) beam longitudinal bars; (b) column longitudinal bars.

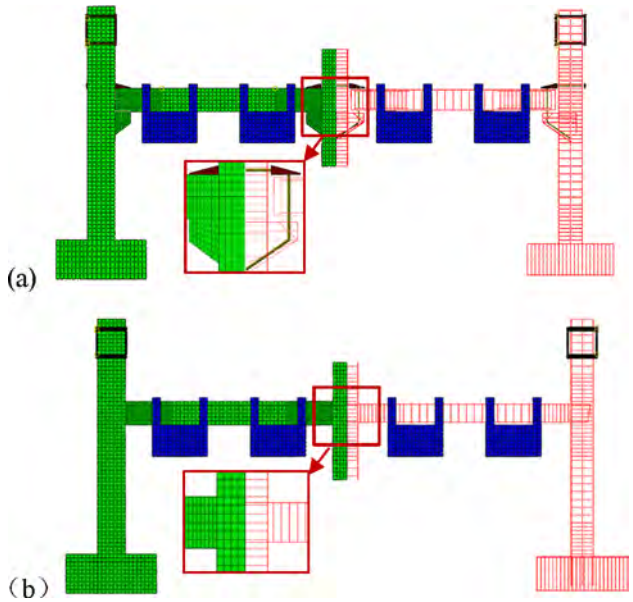

Fig. 20. Analysis elements of reinforcement and concrete: (a) PC specimen; (b) RC specimen.

was chosen as 25 mm for the joint regions and 50 mm for the other regions (along the beam length). Dowel bars and steel angle cleats were modelled by the solid element (C3D8R) to accurately estimate the stress distribution. To address the fact that the perfect bond between the concrete and reinforcement overestimated the bearing capacity, the interface between the reinforcement and surrounding concrete in the beam and column was modelled by an embedded constraint as proposed by Othman and Marzouk [47].

5.2. Boundary conditions

Fixed boundary conditions were applied to footings so as to restrict deformation. A spring constraint was used at the pin support on the top of exterior columns, with a stiffness value of 10 kN/mm based on the test results. A tie constraint was considered at the interaction surface of the dowel bars and high-strength bolts with the steel angle cleats. Friction behaviour between different parts in contact with each other was modelled using an isotropic penalty friction formula, and a friction coefficient of 0.40 was applied to define the friction behaviour in the tangential direction [48–50]. Hard contact was utilized to define the pressure behaviour of the contact interaction in the normal direction [48], and the load baskets were simulated by a rigid body for computational efficiency.

5.3. Material models

The uniaxial stress-strain relationship of concrete prescribed in GB 50010-2010 [38] was used for concrete (Fig. 21(a)). The compressive strength of concrete was measured in the test, in which the elastic modulus, Poisson's ratio, and density were 3×10^4 N/mm^2, 0.2, and 2.4×10^3 kg/m^3, respectively. A Concrete damage plasticity (CDP) model was adopted to consider the nonlinear behaviour, stiffness degradation, and strain rate effect on the material property, which was coupled with fracture energy to ensure mesh-size independent results [47]. The CDP model modifies the yield surface in the deviatoric plane to consider different yield stresses in tension and compression by using a shape parameter (K_c), while the dilation angle (Ψ) is used for plastic flow behaviour. Plastic potential eccentricity (ϵ) increases the dilation angle. The ratio of the biaxial stress to uniaxial stress (σ_{b0}/σ_{c0}) is considered to describe the material state under multi-axial stress. In this study, the corresponding parameters were defined as $K_c = 0.6667$, $\Psi = 38$, $\epsilon = 0.1$, and $\sigma_{b0}/\sigma_{c0} = 1.16$ in accordance with the values used

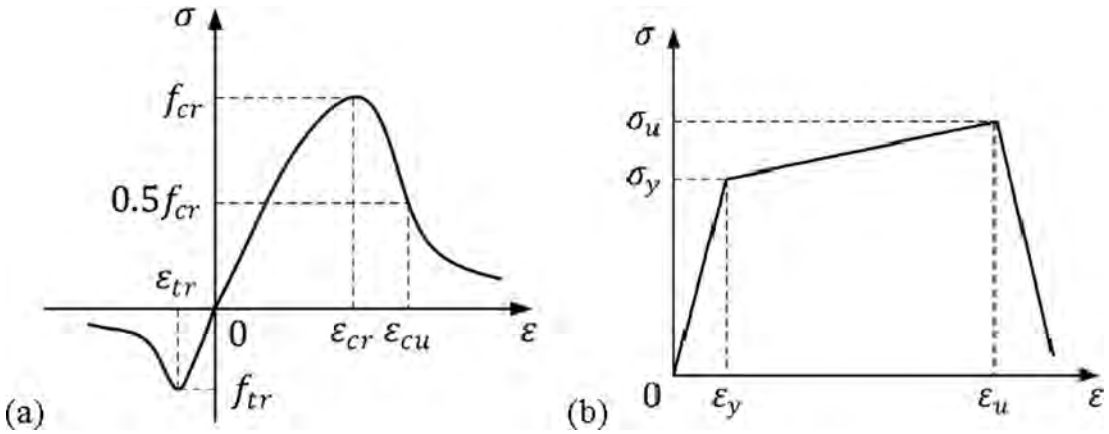

Fig. 21. Stress-strain relationship of materials: (a) concrete; (b) longitudinal bar.

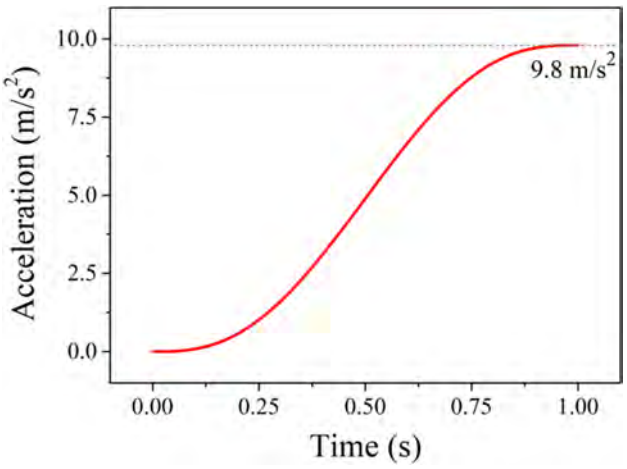

Fig. 22. Gravity loading procedure.

by Genikomsou and Polak [50]. To address strength hardening after yielding and strength degradation after fracture, the trilinear isotropic hardening model was used for longitudinal bars (Fig. 21(b)). The stress-strain relationship of both the high-strength bolts and steel angle cleats was represented by the bilinear isotropic hardening model. The elastic modulus, Poisson's ratio, and density were 2×10^5 N/mm^2, 0.3, and 7.8×10^3 kg/m^3, respectively.

5.4. Loading procedure

The loading procedure for the test was carried out in two steps: the beam was loaded incrementally to simulate the actual loading state; and then the mid-column was suddenly released to simulate the column loss scenario (the axial force of the mid-column was reduced for 0.02 s). Explicit Dynamic in the ABAQUS program was used to solve the non-linear structural analysis of the two specimens, and the loading and release was realized by following the two-step procedure below.

Step 1: A vertical constraint was applied to the bottom of the mid-column, and then the gravity load (i.e. 9.8 m/s^2 as the acceleration of gravity) was slowly applied by extending the loading period to reduce the effect of impact loading on the quasi-static loading mechanism (Fig. 22).

Step 2: The vertical constraint was removed and the released reaction force at the bottom of the mid-column was obtained with the quasi-static analysis method. The gravity load remained unchanged to simulate the static load effect, while the reaction force was reduced to zero in accordance with the test's measured release period.

5.5. Model calibration

In a series of loading procedures, irreversible damage during each loading stage would be accumulated in the multi-stage loading procedure. However, for ease of calculations, each dynamic loading was applied to a new analysis model without residual damage caused by former dynamic loading in the *ABAQUS* program. A damage index test/prediction (T/P) ratio was defined by comparing the structural responses of the maximum deflection under the same loading procedure to evaluate the specimen damage level.

In the PC specimen, the mid-column deflection under the 1st load test was calibrated by FEA (Fig. 23(a)). The prediction agreed well with the test result, and the difference of the peak deflection and natural

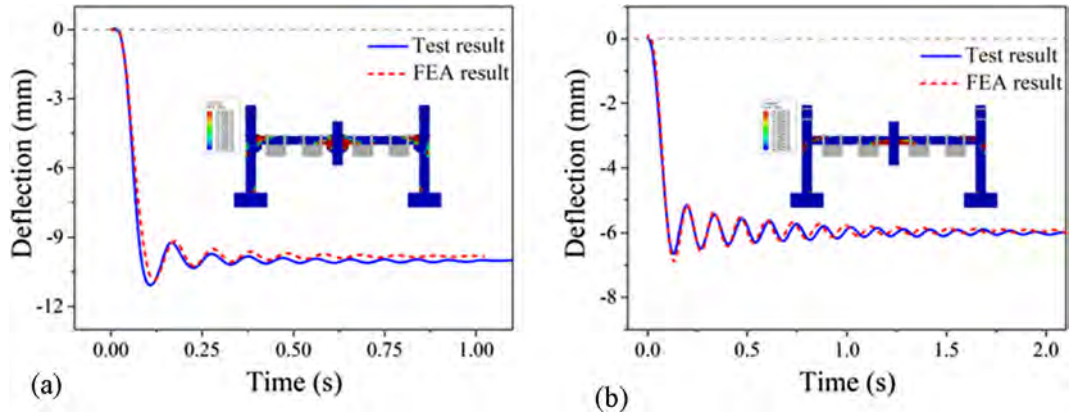

Fig. 23. Comparison between test and FEA results: (a) PC specimen under the 1st load step; (b) RC specimen under the 2nd load step.

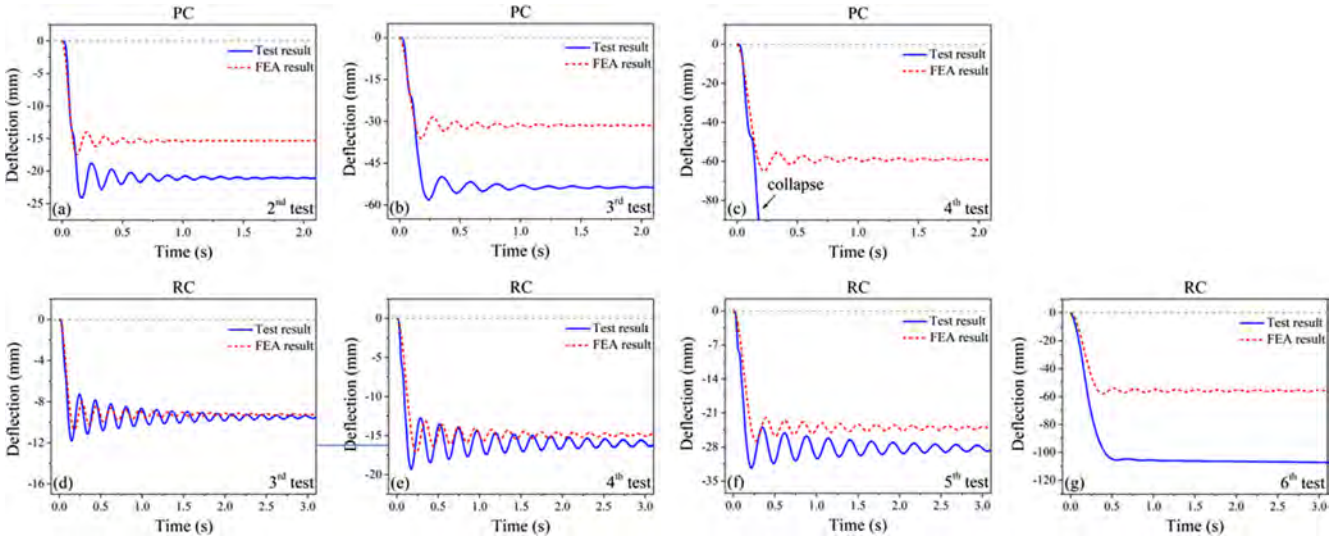

Fig. 24. Analysis results according to load level: (a)–(c) PC specimen; (d)–(g) RC specimen.

Table 5
Comparison of the test results and predictions.

Test ID	Type	Peak deflection			Natural period		
		Test (mm)	Prediction (mm)	T/P	Test (s)	Prediction (s)	T/P
1st	PC	−11.1	−10.9	1.02	0.100	0.110	0.91
	RC	−2.2	–	–	0.090	–	–
2nd	PC	−24.1	−17.5	1.38	0.158	0.148	1.07
	RC	−6.6	−6.9	0.96	0.137	0.138	0.99
3rd	PC	−58.1	−36.3	1.60	0.218	0.185	1.18
	RC	−11.8	−10.7	1.10	0.190	0.181	1.05
4th	PC	–	−64.9	–	–	0.215	–
	RC	−19.2	−17.2	1.12	0.226	0.210	1.08
5th	PC	–	–	–	–	–	–
	RC	–32.3	−26.8	1.21	0.264	0.240	1.10
6th	PC	–	–	–	–	–	–
	RC	−105.5	−58.0	1.82	0.303	0.263	1.15

period was about 2.0% and 7.1%, respectively; similar damage occurred in the corbel and beam-column joint. As the dynamic response for the RC specimen was not significant in the test result under the 1st load step, the test result under the 2nd load step was compared with the prediction (Fig. 23(b)). The prediction agreed well with the test result, and the difference of the peak deflection and natural period was about 3.8% and 4.5%, respectively.

5.6. Analysis results

Fig. 24 and Table 5 show the deflections of the mid-column and the natural periods of the specimens. As the damage increased in the specimens, the discrepancy between the test results and predictions increased. When the released mid-column was moved upward to the original location after the dynamic loading test, the gap at the joint interface was not completely closed due to residual damage. For this reason, the discrepancy was significantly increased in the PC specimen as the dynamic loading increased. Thus, the difference between the test results and predictions can be regarded as a residual damage index. In the PC specimen, the T/P ratio of the peak deflection ranged from 1.02 to 1.60, and the natural period ratio ranged from 0.91 to 1.18. In the RC specimen, the peak deflection ratio ranged from 0.96 to 1.82, and the natural period ratio ranged from 0.99 to 1.15.

5.7. Final failure load and mode estimation

Another purpose for conducting a dynamic test on the large-scale sub-assemblage, was to attain the structural resistance at failure state. After the RC and PC FE models have been calibrated, the analysis model can be further utilized to estimate the weight suspended along the beam by using one free-fall load. After the trial and error calculation, the load for final collapse was estimated as 249.4 kN (60.35 kN weight in each basket) for the RC specimen and 148.16 kN (37.04 kN weight in each basket) for the PC specimen. Fig. 25 shows the predictions of the failure pattern of RC and PC structures. In the RC specimen, cracks and spalling of concrete occurred along the beam, while in the PC specimen concrete damage mainly accumulated near the end-joints and corbels.

6. Discussion

(1) In order to investigate the dynamic behavior of PC and RC moment frames, comparable static tests [46] were conducted for these two specimens using the same reaction frame. Thus, the dynamic load resistance of these two specimens could be estimated according to

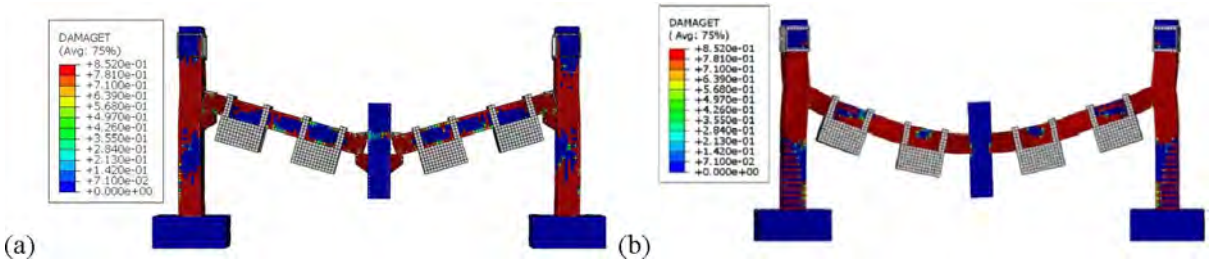

Fig. 25. Predictions of failure pattern: (a) PC specimen; (b) RC specimen.

prior knowledge obtained from the static test. The measured load resistance and the failure mode of the RC and PC specimens under static loading would guide the load weight preparation and specimen failure prevention in the dynamic test.

(2) Since an accurate pre-load for collapse cannot be determined from one free-fall load in the large-scale dynamic loading tests, several load steps were considered by increasing the loading weight on the two beams gradually. The damage caused by the former load step would be accumulated and decrease the load-carrying capacity in the next load step. Thus, the final collapse load was affected by both the load magnitude and the number of load steps. The calibrated FE model can provide an alternative way to estimate the pre-load, which causes the specimen to collapse from one free-fall load.

(3) Both the static and dynamic loading test results indicate that the RC specimen is more rigid than the PC specimen. In the dynamic loading test, the PC specimen exhibited the larger deflection, vibration amplitude, and natural period than those of the RC specimen. This was inconsistent with the static loading test results because of the lower vertical stiffness in the assembled PC specimen showing corbel damage in a large deflection. In the semi-rigid connection, the dowel bar and corbel are suggested to be strengthened to avoid early failure of the connection at CAA, which makes the connection more flexible in CTA.

(4) An interesting failure mode occurred at the 6th step in the RC specimen. The unexpected collapse of the RC specimen appeared without warning after 20 min under sustained load, and the numerical analysis could barely distinguish the sustained stage. Such phenomenon may be attributed to the time-dependent property of concrete at the point of transition from CAA to CTA; this has not been reported in existing studies. The time dependent collapse provides further guidance when evaluating the evacuation time during building collapse.

7. Conclusion

This study performed dynamic loading tests on two half-scale PC and RC moment sub-structures to investigate the progressive collapse performance. For the PC specimen, the beam-column connection was fully assembled using dowel bars embedded in a corbel, and steel angle cleats applied to the connection. The mid-column was suddenly removed under a series of load steps. The structural performance including the load-carrying capacity, deflection, lateral displacement, failure modes, crack distribution, and rebar strains was evaluated. The main conclusions are summarized as follows.

(1) Under dynamic loading, the PC specimen collapsed at the 4th load step using a distributed load of 133.4 kN, and the pre-released load in the mid-column was approximately 81.1 kN. However, the RC specimen failed at the 6th load step using a distributed load of 173.4 kN, and the pre-released load reached 114.3 kN, which was a greater progressive collapse performance than that of the PC specimen.

(2) As the dynamic loading increased, the deflection, response time, and natural period of the PC specimen were larger than those of the RC specimen. This result indicates that the stiffness of the RC specimen is greater than that of the PC specimen due to the better structural integrity of the connection in the RC specimen.

(3) The longitudinal bars of the beam/column did not yield, while a part of the U-shaped bars of the beam-end yielded after the PC specimen collapsed. In the RC specimen, however, the longitudinal bars of the beam yielded and a part of the column bars yielded at CAA. This indicates that the materials of the RC specimen are more effectively used than those of the PC specimen under the same dynamic loading.

(4) CAA was generated in both specimens. The load-carrying capacity of the RC specimen at CAA was approximately 1.4 times that of the PC specimen. The reliable resistance mechanism of CTA was developed in the RC specimen, but not developed in the PC specimen due to shear failure of the dowel bars after CAA was terminated, which induced collapse of the PC specimen. Thus, the use of high-strength or larger diameter dowel bars is recommended to improve the structural performance of PC substructures.

(5) Finite element analysis was performed by the *ABAQUS* program to investigate the structural performance of test specimens. The analysis results agreed well with the test results including the deflection history of the mid-column and crack pattern. However, since residual damage was not considered in the analysis model, the prediction was underestimated at large dynamic loadings. By using the calibrated model to estimate the weight suspended along the beam using one free-fall load, the load for final collapse was estimated as 249.4kN for the RC specimen and 148.16kN for the PC specimen.

It should be noted that only one set of test specimens (one PC substructure and one RC substructure) were tested in this study. In order to evaluate the progressive collapse performance of PC substructures, further research is required under various design and load conditions.

CRediT authorship contribution statement

Yun Zhou: Methodology, Writing - original draft, Visualization, Project administration. **Xiang Hu:** Investigation, Data curation. **Yilin Pei:** Investigation, Formal analysis. **Hyeon-Jong Hwang:** Methodology, Validation, Data curation, Writing - review & editing, Visualization. **Taiping Chen:** Investigation, Formal analysis. **Weijian Yi:** Conceptualization. **Lu Deng:** Supervision.

Declaration of Competing Interest

The authors declare that they have no conflict of interest.

Acknowledgements

The authors sincerely appreciate the funding support provided by the National Natural Science Foundation of China (NSFC) (No. 51878264), the National Key Research and Development Program of China (Nos. 2016YFC0701400, 2016YFC0701308), and the Key Research and Development Program of Changsha City (kq1801010).

Appendix A. Supplementary material

Supplementary data to this article can be found online at https://doi.org/10.1016/j.engstruct.2020.110675.

References

[1] ASCE Standard. Minimum design loads for buildings and other structures. Washington, D.C.; 2002.
[2] Department of Defence (DOD). Design of buildings to resist progressive collapse. Washington, D.C.; 2013.
[3] Ellingwood BR. Mitigating risk from abnormal loads and progressive collapse. J Perform Constr Facil 2006;20(4):315–23.
[4] Hong JK, Kang TH-K. Computing in protection engineering: CFD analysis of blade fragment impact on concrete wall. J Struct Integrity Maint 2018;3(4):210–6.
[5] Stinger SM, Orton SL. Experimental evaluation of disproportionate collapse resistance in reinforced concrete frames. ACI Struct J 2013;110(3):521–30.
[6] Xu M, Gao S, Guo LH, Fu F, Zhang SM. Study on collapse mechanism of steel frame with CFST-columns under column-removal scenario. J Constr Steel Res 2018;141:275–86.
[7] Breccolotti M, Gentile S, Tommasini M, Materazzi AL, Bonfigli MF, Pasqualini B, et al. Beam-column joints in continuous RC frames: comparison between cast-in-situ and precast solutions. Eng Struct 2016;127:129–44.
[8] Ersoy U, Tankut T. Precast concrete members with welded plate connections under reversed cyclic loading. PCI J 1993;38(4):94–100.
[9] Precast Prestressed Concrete Institute (PCI). PCI design handbook, 7th ed.; 2010.

[10] Vidjeapriya R, Jaya KP. Behaviour of precast beam-column mechanical connections under cyclic loading. J Perform Constr Facil 2012;13(2):233–45.
[11] Lacerda MM, Silva TJ, Alva GM, Lima MC. Influence of the vertical grouting in the interface between corbel and beam in beam-to-column connections of precast concrete structures: an experimental analysis. Eng Struct 2018;172:201–13.
[12] Al-Salloum YA, Alrubaidi MA, Elsanadedy HM, Almusallam TH, Iqbal RA. Strengthening of precast RC beam-column connections for progressive collapse mitigation using bolted steel plates. Eng Struct 2018;161:146–60.
[13] Elsanadedy HM, Almusallam TH, Al-Salloum YA, Abbas H. Investigation of precast RC beam-column assemblies under column-loss scenario. Constr Build Mater 2017;142:552–71.
[14] Nimse RB, Joshi DD, Patel PV. Behavior of wet precast beam column connections under progressive collapse scenario: an experimental study. Adv Struct Eng 2014;6:149–59.
[15] Nimse RB, Joshi DD, Patel PV. Experimental study on precast beam column connections constructed using RC corbel and steel billet under progressive collapse scenario. In: Proceedings of structures congress, Reston, VA; 2015.
[16] Tohidi M, Yang J, Baniotopoulos C. Numerical evaluations of codified design methods for progressive collapse resistance of precast concrete cross wall structures. Eng Struct 2014;76:177–86.
[17] Main JA, Bao YH, Lew HS, Sadek F, Chiatiro VP, Robert SD, et al. An experimental and computational study of precast concrete moment frames under a column removal scenario. NIST TN 2015:1–56.
[18] Kang SB, Tan KH. Behavior of precast concrete beam-column sub-assemblages subject to column removal. Eng Struct 2015;93:95–6.
[19] Kang SB, Tan KH. Progressive collapse resistance of precast concrete frames with discontinuous reinforcement in the joint. J Struct Eng 2017;143(9):04017090.
[20] Qian K, Li B. Performance of precast concrete substructures with dry connections to resist progressive collapse. J Perform Constr Facil 2018;32(2). 04018005-1–14.
[21] Feng DC, Wu G, Lu Y. Numerical investigation on the progressive collapse behaviour of precast reinforced concrete frame subassemblages. J Perform Constr Facil 2018;32(3). 04018027-1–14.
[22] Yu J, Luo LZ, Li Y. Numerical study of progressive collapse resistance of RC beam-slab substructures under perimeter column removal scenario. Eng Struct 2018;159:14–27.
[23] Izzuddin B, Vlassis A, Elghazouli A, Nethercot D. Progressive collapse of multistory buildings due to sudden column loss—Part I: simplified assessment framework. Eng Struct 2008;30:1308–18.
[24] Pham Auh Tuan, Tan Kang Hai, Jun Yu. Numerical investigations on static and dynamic responses of reinforced concrete sub-assemblages under progressive collapse. Eng Struct 2017;149:2–20.
[25] Sasani M, Bazan M, Sagirolu S. Experimental and analytical progressive collapse evaluation of an actual reinforced concrete structure. ACI Struct J 2007;104(6):731–9.
[26] Qian K, Li B. Dynamic performance of RC beam-column substructures under the scenario of the loss of a corner column–Experimental results. Eng Struct 2012;42(12):154–67.
[27] Yu J, Tan KH. Experimental and numerical investigation on progressive collapse resistance of reinforced concrete beam column sub-assemblages. Eng Struct 2013;55:90–106.
[28] Yu J, Rinder T, Stolz A, Tan KH, Riedel W. Dynamic progressive collapse of an RC assemblage induced by contact detonation. J Struct Eng 2014;140(6):04014014.
[29] Orton SL, Kirby JE. Dynamic response of a RC frame under column removal. J Perform Constr Facil 2014;28(4):04014010.
[30] Pham AT, Tan KH. Experimental study on dynamic responses of reinforced concrete frames under sudden column removal applying concentrated loading. Eng Struct 2017;139:31–45.
[31] Qian K, Li B. Dynamic and residual behavior of reinforced concrete floors following instantanesous removal of a column. Eng Struct 2017;148:175–84.
[32] Qian K, Weng YH, Li B. Impact of two columns missing on dynamic response of RC flat slab structures. Eng Struct 2018;177:598–615.
[33] Qian K, Liang SL, Xiong XY, Fu F, Fang Q. Quasi-static and dynamic behaviour of precast concrete frames with high performance dry connections subjected to loss of a penultimate column scenario. Eng Struct 2020;205:110115.
[34] Feng F, Hwang HJ, Yi W. Static and dynamic loading tests for precast concrete moment frames under progressive collapse. Eng Struct 2020;213:110612.
[35] McKay A, Marchand K, Williamson E, Crowder B, Stevens D. Dynamic and nonlinear load increase factors for collapse design and analysis. In: International symposium on the interaction of the effects of munitions with structures (ISIEMS), Orlando, FL; 2007.
[36] McKay A, Marchand K, Diaz M. Alternate path method in progressive collapse analysis: variation of dynamic and nonlinear load increase factors. Pract Period Struct Design Constr 2012;17(4):152–60.
[37] Ferraioli M. Dynamic increase factor for nonlinear static analysis of RC frame buildings against progressive collapse. Int J Civ Eng 2019;17(3):281–303.
[38] Ministry of Housing and Urban-Rural Development of China (MHURDOC). Code for design of concrete structures (GB 50010-2010), Beijing: China Architecture and Building Press; 2010 [in Chinese].
[39] Ministry of Housing and Urban-Rural Development of China (MHURDOC). Code for seismic design of building (GB 50011-2010), Beijing: China Architecture and Building Press; 2010 [in Chinese].
[40] Lu HS, Zhao FX. Site coefficients suitable to China site category. Acta Seismol Sin 2007;29(1):67–76.
[41] PKPM analysis user's manual. Version 4.3.4. Beijing (China): China Academy of Building Research Inc.; 2019. http://www.pkpm.cn.
[42] Liu C, Fung TC, Tan KH. Dynamic performance of flush end-plate beam-column connections and design applications in progressive collapse. J Struct Eng 2016;142:04015074.
[43] Mashhadi J, Saffari H. Effects of postelastic stiffness ratio on dynamic increase factor in progressive collapse. J Perform Constr Facil 2017;31(6):04017107.
[44] Clough RW, Penzien J. Dynamics of structures. New York: McGraw-Hill; 1993.
[45] Chopra AK. Dynamics of structures: theory and applications to earthquake engineering. New Jersey: Prentice-Hall; 1995.
[46] Zhou Y, Chen TP, Pei YL, Hwang HJ, Hu X, Yi WJ, et al. Static load test on progressive collapse resistance of fully assemble d precast concrete frame structure. Eng Struct 2019;200:109719.
[47] Othman H, Marzouk H. Finite-element analysis of reinforced concrete plates subjected to repeated impact loads. J Struct Eng 2017;143(9):04017120.
[48] Wriggers P. Computational contact mechanics. Berlin: Springer; 2006.
[49] ABAQUS analysis user's manual. Version 6.13-1. ABAQUS Inc.; 2013.
[50] Genikomsou AS, Polak MA. Finite element analysis of punching shear of concrete slabs using damaged plasticity model in ABAQUS. Eng Struct 2015;98:38–48.